Visualization of hydrogen atoms in a perdeuterated lectin-fucose complex reveals key details of protein-carbohydrate interactions

Lukas Gajdos, Matthew P Blakeley, Atul Kumar, Michaela Wimmerová, Michael Haertlein, V. Trevor Trevor Forsyth, Anne Imberty, Juliette M Devos

Article

Structure

Visualization of hydrogen atoms in a perdeuterated lectin-fucose complex reveals key details of protein-carbohydrate interactions

Graphical abstract

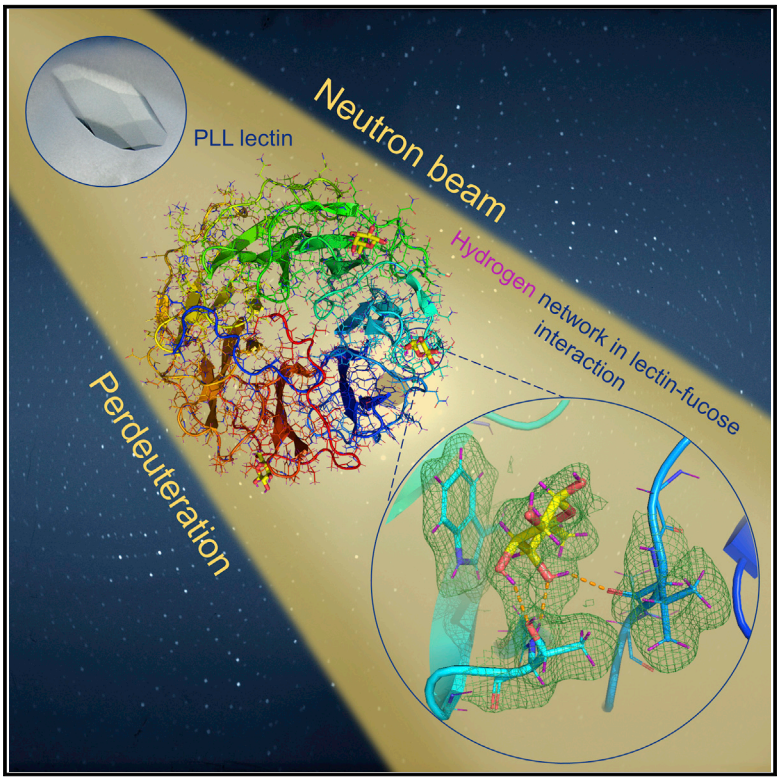

Highlights

- Joint X-ray/neutron structure of bacterial lectin in apo and complex form
- Perdeuterated lectin and sugar improve the quality of neutron density maps
- Fucose methine and methyl groups are involved in CH-π interactions with tryptophan
- Room temperature data avoid glycerol-induced alternate loop conformations

Authors

Lukas Gajdos, Matthew P. Blakeley, Atul Kumar, ..., V. Trevor Forsyth, Anne Imberty, Juliette M. Devos

Correspondence

anne.imberty@cermav.cnrs.fr (A.I.), devosj@ill.fr (J.M.D.)

In brief

Lectins from bacteria interact with sugars on the host surface. Gajdos et al. use joint X-ray/neutron macromolecular crystallography to visualize this lectin/fucose complex. The study highlights hydrogen bond networks, the involvement of water molecules, and key contacts between the apolar face of fucose and the aromatic rings of tryptophan.

Gajdos et al., 2021, Structure *29*, 1–11
July 1, 2021
https://doi.org/10.1016/j.str.2021.03.003

CellPress

Structure

CellPress
OPEN ACCESS

Article

Visualization of hydrogen atoms in a perdeuterated lectin-fucose complex reveals key details of protein-carbohydrate interactions

Lukas Gajdos,[1,2,3] Matthew P. Blakeley,[4] Atul Kumar,[5,6,7] Michaela Wimmerová,[5,6] Michael Haertlein,[1,2] V. Trevor Forsyth,[1,2,8] Anne Imberty,[3,9,10,*] and Juliette M. Devos[1,2,*]

[1]Life Sciences Group, Institut Laue-Langevin, 38000 Grenoble, France
[2]Partnership for Structural Biology (PSB), 38000 Grenoble, France
[3]Université Grenoble Alpes, CNRS, CERMAV, 38000 Grenoble, France
[4]Large Scale Structures Group, Institut Laue-Langevin, 38000 Grenoble, France
[5]CEITEC, Masaryk University, 625 00 Brno, Czech Republic
[6]NCBR, Faculty of Science, Masaryk University, 625 00 Brno, Czech Republic
[7]Institute of Parasitology, Biology Centre of the Czech Academy of Sciences, České Budějovice, Czech Republic
[8]Faculty of Natural Sciences, Keele University, ST5 5BG Staffordshire, UK
[9]Twitter: @AnneImberty
[10]Lead contact
*Correspondence: anne.imberty@cermav.cnrs.fr (A.I.), devosj@ill.fr (J.M.D.)
https://doi.org/10.1016/j.str.2021.03.003

SUMMARY

Carbohydrate-binding proteins from pathogenic bacteria and fungi have been shown to be implicated in various pathological processes, where they interact with glycans present on the surface of the host cells. These interactions are part of the initial processes of infection of the host and are very important to study at the atomic level. Here, we report the room temperature neutron structures of PLL lectin from *Photorhabdus laumondii* in its apo form and in complex with deuterated L-fucose, which is, to our knowledge, the first neutron structure of a carbohydrate-binding protein in complex with a fully deuterated carbohydrate ligand. A detailed structural analysis of the lectin-carbohydrate interactions provides information on the hydrogen bond network, the role of water molecules, and the extent of the CH-π stacking interactions between fucose and the aromatic amino acids in the binding site.

INTRODUCTION

Neutron macromolecular crystallography (NMX) provides unique information on the location of hydrogen atoms in proteins and solvent molecules that is rarely obtainable by X-ray crystallography even at high resolution (Blakeley et al., 2015; Eriksson et al., 2013; Woińska et al., 2016). Neutrons are scattered from atomic nuclei with a scattering power that is isotope dependent. Since the neutron scattering lengths of hydrogen and deuterium are of similar magnitudes to the other elements commonly found in proteins, such as carbon, oxygen, and nitrogen, they can be easily visualized in neutron crystallographic analyses (Blakeley et al., 2018). NMX is thus a powerful technique for structural glycobiology where the location of hydrogen atoms is of crucial importance for understanding the interactions between carbohydrates and amino acids that may involve direct and water-bridged hydrogen bonds. To date (December 2020), there are only 175 macromolecular structures deposited in the Protein Data Bank that have been determined using neutron diffraction data. Glycoside hydrolases (Niimura et al., 1997; Wan et al., 2015), lytic polysaccharide monooxygenase (Bacik et al., 2017; O'Dell et al., 2017), and xylose isomerase (Langan et al., 2014) are carbohydrate-processing enzymes that have been extensively studied by neutron diffraction. On the other hand, only two lectins (sugar-binding proteins) have been studied using neutron crystallography, namely concanavalin A (Blakeley et al., 2004; Gerlits et al., 2017; Habash et al., 1997, 2000; Kalb et al., 2000) and galectin-3C (Manzoni et al., 2016, 2018).

Lectins are carbohydrate-binding proteins having no enzymatic activity. They are involved in various physiological and pathological processes, including molecular and cellular recognition and adhesion (Lis and Sharon, 1998). Many pathogenic bacteria use lectins as toxins or adhesins to promote bacterial infection (Beddoe et al., 2010; Moonens and Remaut, 2017) and the detailed knowledge of their binding site has been used in the design of anti-adhesive compounds, some of them now in preclinical study (Mousavifar et al., 2018).

Photorhabdus laumondii (formerly *P. luminescens*) is a bioluminescent rod-shaped Gram-negative bacterium that lives in a mutualistic relationship with entomopathogenic nematodes from the genus *Heterorhabditis* (Machado et al., 2018; Waterfield et al., 2009). This species can also adopt an alternative lifestyle in the soil, with positive influence on plant rhizosphere (Regaiolo et al., 2020). *P. laumondii* produces several lectins; three of them, PLL (Kumar et al., 2016), PLL2 (Fujdiarová et al., 2020), and PLL3 (Faltinek et al., 2019) having similar in sequences,

Please cite this article in press as: Gajdos et al., Visualization of hydrogen atoms in a perdeuterated lectin-fucose complex reveals key details of protein-carbohydrate interactions, Structure (2021), https://doi.org/10.1016/j.str.2021.03.003

Table 1. Room temperature X-ray and neutron data collection and structure refinement statistics for the H/D-exchanged apo PLL and D-PLL/fucose-d_{12} complex

	H/D-PLL	D-PLL
Data collection	Apo	Fucose-d_{12}
Neutrons		
Instrument	LADI-III	LADI-III
Wavelengths (Å)	3.1–4.1	3.07–4.05
Detector	Image plate	Image plate
Resolution (Å)	39–2.20 (2.32–2.20)	46–2.20 (2.32–2.20)
Space group	I222	I222
Unit cell parameters		
a, b, c (Å)	72.7, 89.3, 159.4	72.7, 89.2, 159.2
α, β, γ (°)	90, 90, 90	90, 90, 90
R_{merge} (I) (%)	18.1 (45.8)	16.3 (32.6)
R_{pim} (I) (%)	13.2 (26.1)	8.3 (16.0)
Mean I/σ(I)	6.2 (2.0)	8.0 (3.4)
Completeness (%)	82.9 (73.5)	84.9 (74.7)
Multiplicity	2.8 (3.0)	4.1 (4.0)
No. of unique reflections	21,855 (2,797)	22,348 (2,822)
Crystal size (mm^3)	0.7	0.5
X-rays		
X-ray source	FIP-BM30A, ESRF	GeniX 3D Cu High Flux (Xenocs), IBS
Wavelength (Å)	0.9796	1.5418
Detector	ADSC Q315r	Mar 345 (marXperts)
Resolution (Å)	46–1.70 (2.02–1.70)	33–1.84 (1.88–1.84)
Unit cell parameters		
a, b, c (Å)	72.7, 89.3, 159.4	72.7, 89.2, 159.2
α, β, γ (°)	90, 90, 90	90, 90, 90
R_{merge} (*I*) (%)	6.4 (77.5)	11.3 (58.2)
R_{meas} (*I*) (%)	7.5 (90.8)	11.8 (64.0)
CC½ (%)	99.8 (63.3)	99.8 (82.7)
Mean I/σ(I)	12.4 (1.65)	14.7 (3.1)
Completeness (%)	98.6 (99.7)	100.0 (100.0)
Multiplicity	3.5 (3.5)	11.5 (5.8)
No. of unique reflections	56,577 (4,157)	45,268 (2,766)
Refinement		
R_{work}/R_{free} (%), X-ray	13.5/15.6	12.1/14.0
R_{work}/R_{free} (%), neutron	21.5/24.0	19.1/22.1
No. of atoms (protein)	2,850	2,939
No. of water molecules	340	334
RMSD		
Bond lengths (Å)	0.010	0.010
Bond angles (°)	1.312	1.323
Average B factors ($Å^2$)		
Protein	29.7	34.6
Ligand	–	51.9
PDB:	7BBI	7BBC

Values in parentheses are for the highest-resolution shell. RMSD, root-mean-square deviation.

have been recently characterized and are proposed to play important roles in the complex *Photorhabdus* life cycle. All three lectins bind L-fucose and their monomeric structure folds as a seven-bladed β propeller characteristic of this family of lectins. PLL is a homotetramer with seven putative monosaccharide binding sites per monomer, of which three were occupied by L-fucose

Please cite this article in press as: Gajdos et al., Visualization of hydrogen atoms in a perdeuterated lectin-fucose complex reveals key details of protein-carbohydrate interactions, Structure (2021), https://doi.org/10.1016/j.str.2021.03.003

CellPress
OPEN ACCESS

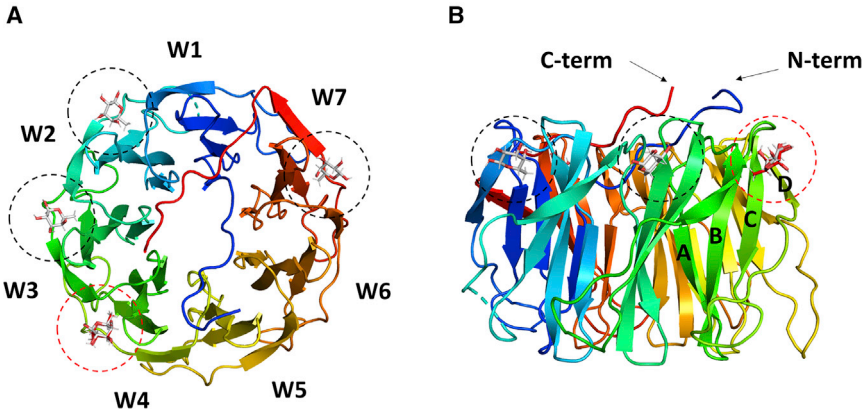

Figure 1. X-ray structure of D-PLL monomer with fucose-binding sites

(A) Top view of the D-PLL monomer (PDB: 7BB4). Four molecules of fucose located between adjacent repeats (W1–W7) are shown in stick representation. Black-circled sites are sites that have been already described. The red-circled site is an additional binding site described here.

(B) Side view of the monomer.

in the X-ray crystal structure (Kumar et al., 2016). The PLL lectin from *P. laumondii* is an excellent model system for the study of lectin/carbohydrate interactions since the binding of fucose involves several hydrogen bonds to the protein side neutron structures chain and main chain atoms, bridged by water molecules, and, very interestingly, hydrophobic contact with two tryptophan residues that involve CH/π dispersion interactions important in protein-carbohydrate complexes (Wimmerová et al., 2012).

To optimize the study of the lectin-carbohydrate interactions using neutron diffraction experiments, it is highly advantageous to perdeuterate (i.e., fully deuterate) both the protein and the ligand, so that all hydrogen atoms are replaced by deuterium. This maximizes the visibility of the coherent neutron diffraction signal (Haertlein et al., 2016) by eliminating the inherently large incoherent scattering from hydrogen. In addition, the negative sign of the coherent neutron scattering length of hydrogen gives rise to cancellation effects in neutron scattering length density maps determined at medium resolutions (~1.6–2.5 Å), which makes it difficult to visualize hydrogen and carbon atoms in -CH_2 groups (Fisher et al., 2014; Koruza et al., 2019). The use of perdeuterated molecules obviates this problem and provides better quality neutron scattering length density maps.

Perdeuterated recombinant proteins are now commonly produced using bacterial and yeast expressions systems that have been adapted to D_2O-based growth medium and a deuterated carbon source (Haertlein et al., 2016; Meilleur et al., 2009). Perdeuterated glycans, on the other hand, are not easily available and only a limited number have been produced via synthetic or enzymatic approaches (Cress et al., 2019; Kent et al., 2015; Sawama et al., 2012). Very few neutron structures of proteins complexed with perdeuterated carbohydrate have been characterized (Kovalevsky et al., 2008, 2010; Langan et al., 2014). Recently, however, we reported the production of perdeuterated L-fucose-d_{12} (Fuc-d_{12}) obtained using a glyco-engineered *E. coli* strain, genetically modified to produce high titers of L-fucose (Gajdos et al., 2020).

Here, we report the neutron and X-ray structures of the apo and fucose-bound PLL lectin from *P. laumondii*. This is, to our knowledge, the first account of a neutron structure of a perdeuterated lectin bound to a perdeuterated monosaccharide, allowing for a precise description of the hydrogen bond network and the π-stacking interactions between the hydrophobic face of fucose and the aromatic rings of amino acids in the binding site.

RESULTS

Neutron diffraction data from PLL that was buffer-exchanged in D_2O (H/D-PLL) in the apo form and from perdeuterated PLL (D-PLL) complexed with perdeuterated fucose (Fuc-d_{12}) were collected from single crystals (volume 0.5–0.7 mm^3) to 2.2 Å resolution (Figure S1). For the joint X-ray/neutron structural refinement, room temperature (RT) X-ray data were collected from the same crystals to resolutions of 1.70 Å (H/D-PLL apo) and 1.84 Å (D-PLL/Fuc-d_{12}), respectively (Tables 1 and S1). In addition, three RT X-ray structures of D-PLL apo, H/D-PLL/H-fucose (commercial L-fucose) and D-PLL/H-fucose complexes as well as one 100 K X-ray structure of D-PLL/H-fucose complex were collected for comparison (Table S2).

Overall structure of D-PLL and comparison of RT and 100 K X-ray structures

The overall X-ray structures of H/D-exchanged PLL and D-PLL consist of a homotetramer of seven-bladed β propellers linked by disulfide bridges (Figure 1). There is only one PLL monomer in the asymmetric unit. It is similar to the previously reported H-PLL (Kumar et al., 2016) and will not be described in details here. The superposition of the RT joint X-ray/neutron refined structures of D-PLL and H/D-PLL gives an overall root-mean-square deviation (RMSD) of 0.17 Å (backbone atoms) indicating that the deuteration did not lead to any significant modifications of the 3D structure and that both structures are comparable. Similar results were obtained after superposition of the 100 K X-ray crystal structures of the H-PLL and D-PLL giving an RMSD of 0.13 Å (backbone atoms).

Interestingly, larger differences were observed when comparing the structures obtained at RT and 100 K, with mean RMSD of 0.64 Å (backbone atoms). After investigation, two clear differences were observed between the RT and 100 K structures of the protein, regardless of its H- or D-form. Differences were visibly pronounced in the short loops connecting β strands C and D of the W1 and W5 repeats, respectively, caused by glycerol molecules that altered their conformations. Specifically, in both short loops, a glycerol molecule is strongly bound to the amino acids via six hydrogen bonds (Figure 2) making the loops shift away from their normal positions observed in the RT structures. All 100 K structures of PLL lectin from the previous study (Kumar et al., 2016), and this work, were collected from crystals soaked in glycerol solution, which served as a cryoprotectant during the crystal cryo-cooling. Glycerol readily binds to the protein with an average of 17

Please cite this article in press as: Gajdos et al., Visualization of hydrogen atoms in a perdeuterated lectin-fucose complex reveals key details of protein-carbohydrate interactions, Structure (2021), https://doi.org/10.1016/j.str.2021.03.003

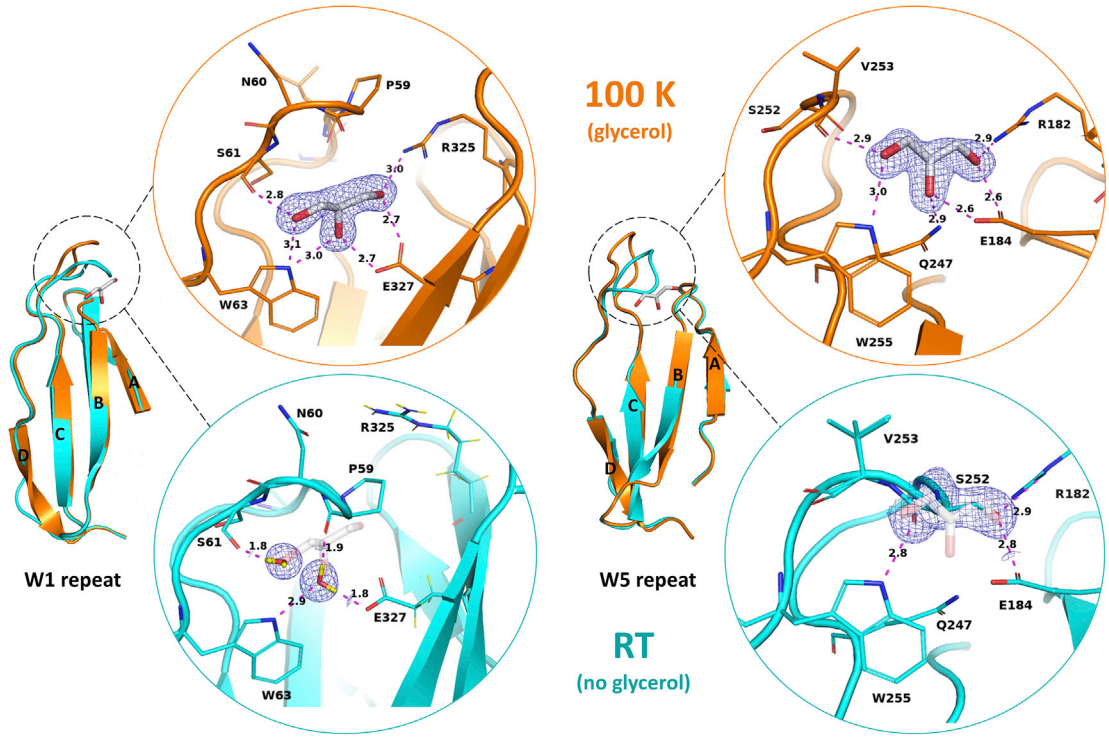

Figure 2. Superposition of 100 K (orange, PDB: 7BB4) and room temperature (cyan, PDB: 7BBC) X-ray structures of repeats W1 and W5 of the D-PLL β propeller. $2mF_o - DF_c$ electron density is shown as a blue mesh and contoured at 1.5σ level

Hydrogen bonds are shown as magenta dashed lines and distances are given in Å. (Top) In the 100 K structure, a glycerol molecule (used as a cryoprotecting agent) binds strongly to the protein changing the native conformation of the short loop between strands C and D of the repeats W1 and W5 observed in the room temperature structure collected from crystals mounted in capillaries. (Bottom) In the RT structure, native conformation of loops is presented. Glycerol molecules (transparent gray sticks) from the 100 K structure are superimposed with the RT structure.

glycerol molecules per monomer for the apo protein and 11 for the fucose-bound complex.

An unexpected difference between X-ray structures at RT and at 100 K is the number of occupied binding sites. In the crystal structure of the H-PLL/H-fucose complex (PDB: 5C9P), three fucose molecules were observed in three binding sites: site II (between W-motifs 1 and 2), III (between W-motifs 2 and 3), and VII (between W-motifs 6 and 7), respectively (Figure 1). Here, we report an additional binding site IV (between repeats W3 and W4) occupied by a fucose molecule in our RT and 100 K X-ray structure, in place of a glycerol molecule in the previously reported structure at 100 K (Figure 3). The fucose molecule could be modeled in a mixture of α/β configurations with occupancies of 54/46. Generally, the fucose is bound in site IV in a similar manner to the other sites (Figure S2). The strongest hydrogen bonds are between the O4 oxygen of L-fucose and the backbone ND of Ala190 and O of Thr168. Fucose is further stabilized via backbone hydrogen bonds of NH (Thr168) to the sugar ring O or O4 oxygen atoms.

Neutron structures and quality of the neutron density map

The use of perdeuterated protein yielded high-quality neutron scattering length density maps (Figure 4A) (hereafter referred to as "neutron maps"). Exchangeable protons could be located without ambiguity in the $2mF_o - DF_c$ neutron map. The deuterium on the amine group of the main chain could be visualized as well as their involvement in hydrogen bonds (Figure 4B). However, the H/D-exchanged protein neutron structure exhibited clear cancellation effects in the $2mF_o - DF_c$ maps, mostly around aliphatic residues (Figure 4A).

The protonation states of the histidine residues could also be unambiguously determined from the analysis of the perdeuterated structure (D-PLL/Fuc-d_{12}). All histidines of the H/D-exchanged apo PLL were protonated on both nitrogen atoms ND1 and NE2 as a result of the low pH of 4.6 used in the crystallization condition In comparison, all but two of the histidine residues were equally protonated in the perdeuterated D-PLL/Fuc-d_{12} crystal (Table 2) grown at a physiological pH (0.1 M sodium potassium tartrate, pH ~ 7). Based on the examination of the $2mF_o - DF_c$ omit neutron map, His155 and His176 were found to be in the neutral NE2-protonated and ND1-protonated tautomeric forms, respectively (Figure 4C). It is noteworthy that none of the histidine residues of the PLL lectin is involved or is in the vicinity of the sugar-binding sites. Further analysis of the neutron structures showed no protonation on any acidic side chains (Asp, Glu).

The $2mF_o - DF_c$ X-ray map for the D-PLL/Fuc-d_{12} complex at 1.85 Å resolution shows clear electron density for the ligand in binding sites II (Figure 5), III, and VII. The fourth binding site described above for the RT X-ray structure is not occupied by the ligand in the neutron structure of the complex. The site is occupied by solvent molecules (Figure S3B) that are also

Please cite this article in press as: Gajdos et al., Visualization of hydrogen atoms in a perdeuterated lectin-fucose complex reveals key details of protein-carbohydrate interactions, Structure (2021), https://doi.org/10.1016/j.str.2021.03.003

CellPress
OPEN ACCESS

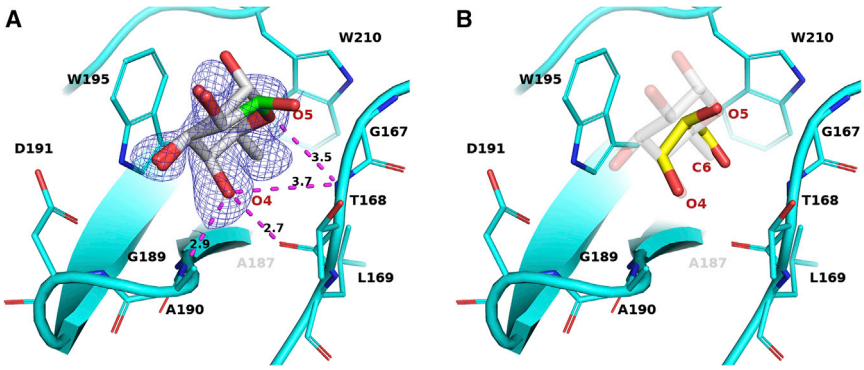

Figure 3. X-ray structure of fucose in the additional binding site IV of D-PLL located between repeats W3 and W4 of the seven-bladed β propeller

(A) $2mF_o - DF_c$ X-ray omit map (blue mesh) around L-fucose is contoured at 0.9σ. The position of fucose O1 atom is modeled in both α (gray) and β (green) configurations. Hydrogen bonds are depicted as magenta dashed lines. All distances are given in Å (PDB: 7BB4).

(B) Superposition of the fucose (transparent gray sticks) and a glycerol molecule (yellow sticks) modeled in apo PLL (PDB: 5C9O). The fucose atom labeling corresponds to the superimposed glycerol oxygen atoms.

observed in the 100 K X-ray structure (PDB: 5C9P). A possible explanation is that this site has a lower affinity for fucose than the other sites, as suggested previously (Kumar et al., 2016). In all sites, fucose could be modeled in both α/β configurations with occupancies of 30/70, in agreement with the population of 30/70 observed by NMR in solution (Ryu et al., 2004). The neutron scattering density around the deuterated fucose molecule is clearly different from the electron density given that the deuterium atoms contribute strongly to the neutron scattering (Figure 5A). As a result, neutron peaks of the methyl group together with deuterium atoms on carbon atoms are visible in the density map and the directionality of the fucose hydroxyl groups could be determined. The map quality is better in binding site II located between blades W1 and W2 of the β propeller.

Hydrogen bonding in the fucose-binding sites

The sugar-binding mode is essentially identical in all binding sites and the orientation of the sugar is similar to the one previously observed in the X-ray structure (Kumar et al., 2016). Only the novel features highlighted by the neutron maps are therefore described here. In site II, the two key fucose hydroxyl groups OD3 and OD4 are involved in direct hydrogen bonds with the protein (Figure S4). The neutron map displays very good continuity of density between fucose O3 and the hydroxyl group of Thr94 (Figure 5B). The neutron structure clarifies the direction of the hydrogen bond, with deuterium on Fuc-O3 pointing toward OG1 of the Thr94 side chain (1.94 Å), while the deuterium on this oxygen goes to the solvent. The Fuc-O4 oxygen atom accepts an H bond from the backbone amine of Thr94 (2.02 Å) clearly observed in the neutron density map while the deuterium of Fuc-O4 points toward the backbone oxygen of Val72 (2.06 Å).

The same hydrogen bond network is observed in site III, with the addition of the ring oxygen O5 accepting one hydrogen bond from the backbone amide of Gly120. Fucose has the same orientation in site VII but the map is of lower quality in this region. Measured distances and angles of hydrogen bonds are presented in Table 3.

The neutron structure also provides insight to the role of water molecules in the ligand binding. In binding site II, one water molecule bridges between Fuc-O1 in β configuration and the protein, with clear density around the two deuterium atoms involved. The Fuc-O1β atom accepts an H bond (1.62 Å) from this water, which in turn accepts another hydrogen bond from the backbone amide of Val72 (2.30 Å). Two additional waters seem to be bridging the interaction of the Fuc-O3 atom and Asp95, although with weak neutron density suggesting higher mobility and weaker coordination.

CD/π interactions observed in the neutron structure

All fucose-binding sites of the PLL lectin are characterized by a conserved tryptophan-tryptophan cross-strand pair whose aromatic planes are directed at a near-right angle (varying from 87° to 115°), creating a cleft to which the fucose is coordinated with interaction from both its hydrophobic face and its methyl group (Figure 5C). The neutron maps highlight the perfect complementarity of shape between the flat surface formed by aliphatic deuterium atoms on C3, C4, and C5 of fucose and the aromatic ring of Trp99 (in site II) resulting in strong CD/π dispersion interactions. The methyl group of fucose is furthermore stabilized by interaction with the second tryptophan residue, Trp114 (in site II). The same interaction is observed in the two other binding sites (Figure S3) in the D-PLL/Fuc-d_{12} structure.

Two selection criteria were chosen for defining CD-π dispersion interactions based on previous studies (Brandl et al., 2001). The first criterion was the closest distance between the fucose carbon atom and the ring center of the π system of a tryptophan residue (d(C*n*-π)) with the cutoff value of 4.5 Å. The second criterion was the angle at the deuterium atom (∠C-D-π) defined as the angle between the deuterium atom and the ring center of the π system of a tryptophan residue with values being ≥120° (Figure S4). To better describe deuterium atoms involved in the CD-π interactions, the indole ring of tryptophan side chains was taken as two separate aromatic rings (benzene and pyrrole) with two geometrical centers. The measured interatomic distances and angles are listed in Table 4.

Analysis of the measured distances and angles shows that up to four CD-π interactions occur in the fucose binding by PLL lectin. Deuterium atoms on C3, C4, C5, and C6 are involved in CD-π stacking interaction in all binding sites with average distances of 3.14, 2.95, 3.29, and 3.15 Å, respectively. In binding site II, the strongest interaction is between D4 and the pyrrole ring of Trp99 (2.85 Å), whereas deuterium atoms on C3 and C5 interact weaker with the benzene part of Trp99 with distances of 3.34 and 3.36 Å, respectively (Figure 5C). Furthermore, the deuterium atom on the fucose methyl group interacts with the pyrrole ring of the second tryptophan residue Trp114 with a distance of 3.27 Å. The binding interactions are the same in the other binding sites (Figure S3).

Please cite this article in press as: Gajdos et al., Visualization of hydrogen atoms in a perdeuterated lectin-fucose complex reveals key details of protein-carbohydrate interactions, Structure (2021), https://doi.org/10.1016/j.str.2021.03.003

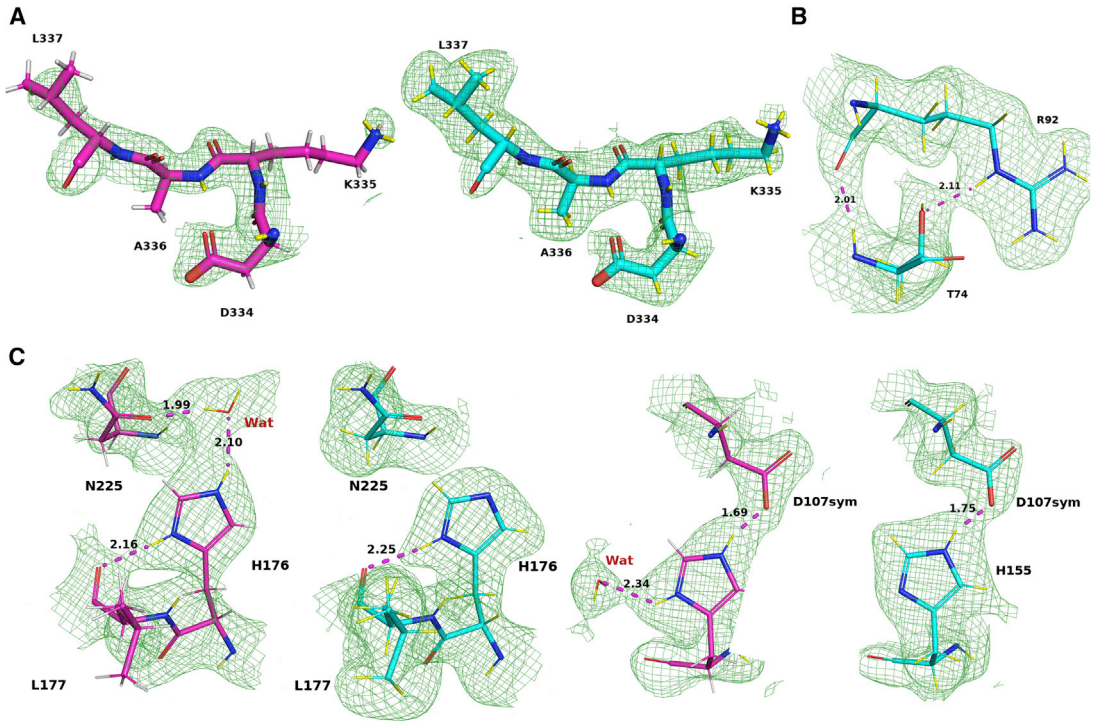

Figure 4. Quality of the neutron scattering length density map

(A) Stick representation and associated neutron density maps of selected residues of the H/D-PLL (magenta sticks) and D-PLL (cyan sticks). Hydrogens atoms are colored white and deuterium atoms are colored yellow. The $2mF_o - DF_c$ neutron density map (green mesh) is contoured at 1σ. The use of perdeuterated protein provides better quality maps than those calculated for the H/D-exchanged protein where interpretation is limited by clear density cancellation effects around the CH groups of the aliphatic amino acids.

(B) Example of a backbone hydrogen bond with a corresponding neutron density.

(C) Comparison of the protonation states of His176 and His155 for the H/D-exchanged apo PLL (magenta sticks) and D-PLL/Fuc-d_{12} (cyan sticks) neutron structures. All distances are measured from a deuterium atom to the acceptor atom and are given in Å.

Water network in the apo (ligand-free) neutron structure

In the apo (ligand-free) neutron crystal structure (2.2 Å resolution), the carbohydrate-binding sites are occupied by three water molecules, which are conserved in all three fucose-binding sites II, III, and VII. The average crystallographic B factors for the three water molecules are similar and rather high (50.7, 57.2, and 53.5 $Å^2$, respectively) suggesting high mobility due to the limited occurrence of hydrogen bonds to the protein. The positions of water oxygen atoms were based on the $2mF_o - DF_c$ electron density map peaks. In the neutron map, the waters form a hydrogen-bonding network creating a continuous density (Figure 6A). The most buried water molecule (Wat1) occupies the position of Fuc-O4 (Figure 6B). This is the most ordered water molecule establishing two hydrogen bonds with the protein. In binding site II, Wat1 oxygen atom accepts an H bond from the backbone amide of Thr94 (2.07 Å), while it donates one deuterium atom to the main chain oxygen of Val72 (2.05 Å). The second deuterium atom of Wat1 is coordinated toward the other water Wat2. The Wat1 water is coordinated in the same fashion in other binding sites (Figure S5).

The two other water molecules are more weakly coordinated and establish hydrogen bonds between them, rather than to the protein. Interestingly, Wat2 occupies positions between C5 and C6 (methyl group) of fucose, which is unconventional for sugar-binding proteins. Usually waters occupy positions of oxygen atoms of the sugar hydroxyl group mimicking the hydrogen bonding of the saccharide. PLL binding sites show hydrophobic character, suggesting that the water molecules might be stabilized by nonconventional lone-pair$\cdots\pi$ or O-H$\cdots\pi$ interactions with the aromatic ring of the tryptophan (Durec et al., 2018).

DISCUSSION

Protein-carbohydrate interactions are involved in many important physiological and pathological processes, including cell

Table 2. Protonation states of histidine residues observed in the neutron crystal structures

State	H51	H80	H100	H148	H155	H176	H196	H203	H244	H298	H339
Apo	both	both	both	both	both	both	both	both	both	ND	both
Fucose	both	both	both	both	NE2	ND1	both	both	both	ND	both

Please cite this article in press as: Gajdos et al., Visualization of hydrogen atoms in a perdeuterated lectin-fucose complex reveals key details of protein-carbohydrate interactions, Structure (2021), https://doi.org/10.1016/j.str.2021.03.003

CellPress
OPEN ACCESS

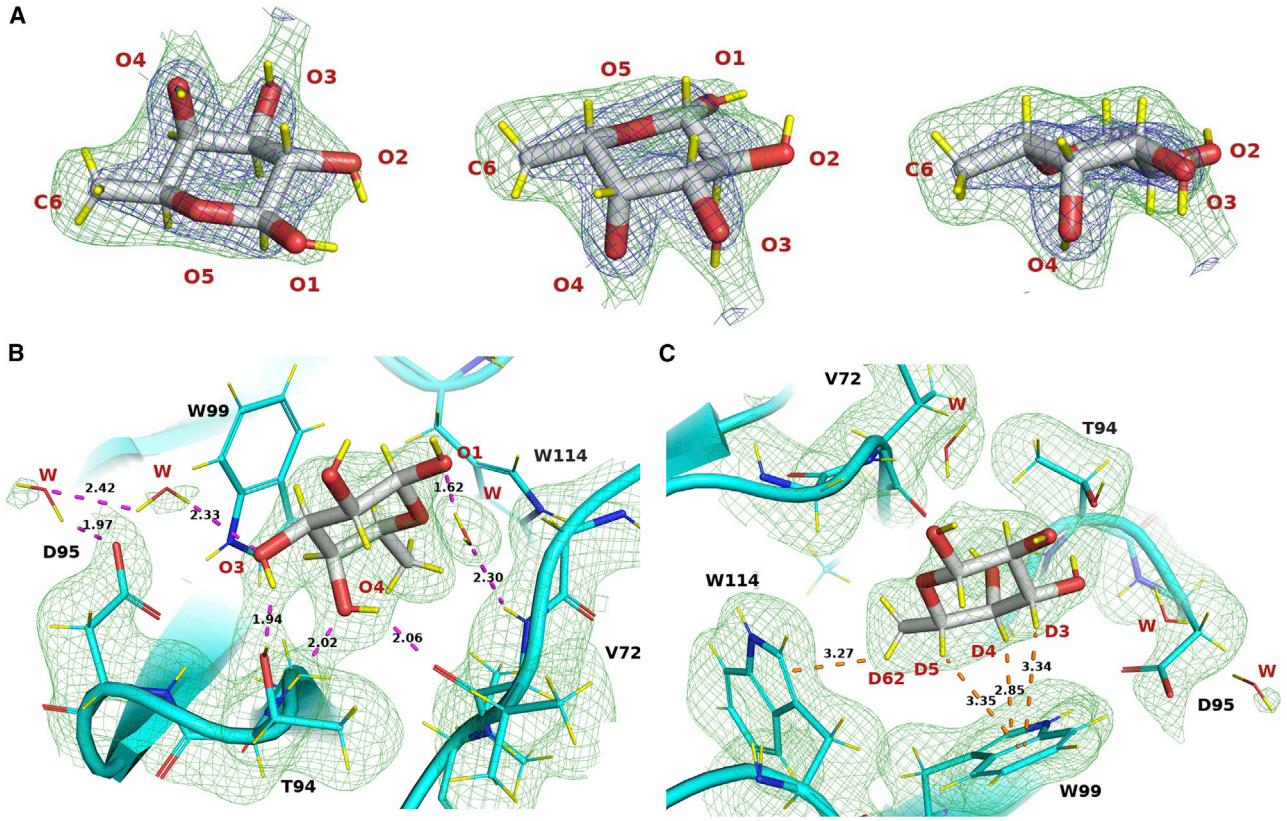

Figure 5. Perdeuterated PLL lectin binding site with bound perdeuterated L-fucose

(A) Electron and neutron density around perdeuterated fucose. Three different views of perdeuterated L-fucose (gray sticks) in the binding site II of the D-PLL/Fuc-d_{12} complex (only β configuration is displayed for the O1 atom). Deuterium atoms are colored yellow. The $2mF_o - DF_c$ neutron scattering length density (green mesh) is contoured at 1σ and the $2mF_o - DF_c$ electron density (blue) is contoured at 2σ level.

(B) Hydrogen-bonding network around the fucose-d_{12} molecule in site II. The $2mF_o - DF_c$ neutron scattering length density (green mesh) is shown at a 1σ counter level. The L-fucose is shown as thick gray sticks and the protein is shown as thin cyan sticks. Deuterium atoms are shown as yellow sticks. Hydrogen bonds are shown as magenta dashed lines.

(C) View rotated by 180° around the axis perpendicular to the panel to highlight the CD-π interactions between the nonpolar face of the fucose and the aromatic amino acids in site II. CD-π dispersion interactions are shown as orange dashed lines with distances (Å) between C and D and the benzene/pyrrole ring centroid of the relevant tryptophan residue.

trafficking, fertilization, immune response, cell adhesion, or viral and bacterial infections. Lectins bind to carbohydrates mainly via hydrogen bonds, either directly or through water bridges, as well as via CH-π dispersion interactions. These latter can sometimes be the main driving force behind lectin-carbohydrate interactions (Asensio et al., 2013; Houser et al., 2020). The molecular mechanisms behind these interactions are predominantly studied at the atomic level by X-ray crystallography, which can locate individual hydrogens only at subatomic resolution (Takaba et al., 2019). The focus of this study was to describe lectin-carbohydrate interactions by NMX as it provides unique and needed information on exact positions of hydrogen atoms involved in the sugar recognition.

In this study, we report the first neutron structure, to our knowledge, of a bacterial lectin in its unbound and in a ligand-bound form. So far, two lectins have been studied by NMX, a glucose/mannose-specific lectin concanavalin A from plants (Blakeley et al., 2004; Gerlits et al., 2017; Habash et al., 1997, 2000; Schirò et al., 2012) and a human galactose-specific galectin-3C (Manzoni et al., 2016, 2018).

We compare RT jointly refined X-ray/neutron crystal structures of H/D-exchanged PLL lectin in its apo form and the perdeuterated D-PLL/Fuc-d_{12} complex. No large differences were observed between H and D forms of PLL lectin concluded that perdeuteration did not affect the native state of the protein. Some differences were observed for the 100 K and RT X-ray structures of PLL lectin regardless of its H/D state. We observed changes in conformation of short loops in repeats W1 and W5 that were caused by a bound glycerol used as a cryoprotectant in the 100 K structures. Moreover, a fucose molecule in our RT and 100 K structure of D-PLL lectin (PDB: 7B7C and 7BB4, respectively) occupies an additional binding site IV between repeats W3 and W4 of the β propeller. This site has not been described yet as it was occupied by water molecules (PDB: 5C9P) or a glycerol molecule (PDB: 5C9O) in 100 K X-ray crystal structures (Kumar et al., 2016). Even though most of the X-ray structures are solved from data collected at cryogenic conditions (100 K), RT structures (293 K) can often provide more relevant information on the protein conformation state and ligand binding since they are closer to physiological conditions and

Please cite this article in press as: Gajdos et al., Visualization of hydrogen atoms in a perdeuterated lectin-fucose complex reveals key details of protein-carbohydrate interactions, Structure (2021), https://doi.org/10.1016/j.str.2021.03.003

Table 3. Measured distances and angles of hydrogen bonding interactions between perdeuterated L-fucose and PLL lectin based on the jointly refined X-ray/neutron crystal structure (D-PLL/Fuc-d_{12})

Site	Donor	Acceptor	Distance (Å)	Angle (°)
II	Fuc-O4D	Val72-O	2.06	129.7
	Thr94-ND	Fuc-O4	2.02	158.3
	Fuc-O3D	Thr94-OG1	1.94	153.2
	W309-OD	Fuc-βO1	1.62	163.5
III	Fuc-O4D	Gly120-O	1.88	145.8
	Ser142-ND	Fuc-O4	2.05	166.8
	Fuc-O3D	Ser142-OG	2.13	129.1
	Gly120-ND	Fuc-O5	2.21	144.6
VII	Fuc-O4D	Ile311-O	1.95	165.7
	Leu333-ND	Fuc-O4	2.16	166.0

may avoid artifacts caused during cryo-cooling of protein crystals as observed by others (Maeki et al., 2020).

The RT X-ray/neutron structure of the perdeuterated complex deciphered the hydrogen bond network involved in the fucose-binding sites, with clear directionalities of fucose hydroxyl groups observed in the neutron map. Fuc-OD4 is the key fucose hydroxyl group in the PLL sugar recognition as it makes two strong and well-defined hydrogen bonds with the protein backbone atoms in all binding sites. Fucose is further stabilized by another hydrogen bond between Fuc-OD3 and a polar side chain in sites II and III, while in sites IV and VII amino acids in this position have nonpolar character, which precludes formation of this hydrogen bond. This is consistent with the neutron map quality that is of lower quality in binding site VII.

Moreover, deuterium atoms of the perdeuterated L-fucopyranose ring can be seen clearly in the neutron density. This is due to the contribution of the deuterium scatterers with a positive neutron scattering length so that the positions of all deuterium atoms can be unambiguously determined. To date, only a couple of neutron structures have used perdeuterated monosaccharides, which were all chemically synthetized (Kovalevsky et al., 2008; Langan et al., 2014). In our study, we used a perdeuterated sugar produced via biosynthetic pathways in glyco-engineered *E. coli* bacteria that was reported recently (Gajdos et al., 2020). The use of hydrogenated sugars can lead to cancellation effects in the neutron maps, mainly around CH_2 groups, which might make interpretation of maps challenging. Here, no cancellation effects were observed and a strong peak of the fucose methyl group could be clearly seen in the neutron scattering length density map. The fucose methine and methyl groups at C3-C5 and C6, respectively, are involved in the CD/π interactions with the tryptophan side chains. The average distances between the deuterium atom and the ring centroid of the relevant tryptophan residue are in the range 2.62–3.49 Å, which is in agreement with the recently published analysis of CH-π interactions based on the 3D structures of protein-carbohydrate complexes deposited in the PDB (Houser et al., 2017, 2020). Experimentally determined structures of CH-π dispersion interactions are necessary for a better understanding of the nature and physics behind the dispersion forces involved in the protein-carbohydrate interactions. These can be used in the quantum chemical calculations of interaction energies, which could eventually improve structure-based drug design of new inhibitors.

Interestingly, in the RT X-ray/neutron structure of the unbound PLL lectin, three water molecules were observed at the positions of fucose O4, C5, and C6 atoms. The strongest neutron peak was for the water located on the position of Fuc-OD4, which is the most ordered water molecule in all binding sites. The other two waters seem to be less coordinated with only one hydrogen bond to the protein. It is possible that these water molecules

Table 4. Experimentally determined geometrical parameters of CD-π interactions between perdeuterated L-fucose and aromatic amino acids in the binding sites of the perdeuterated PLL lectin based on the X-ray/neutron jointly refined crystal structure

		d(C*n*-π) (Å)		d(D*n*-π) (Å)		∠(C*n*-D*n*-π) (°)	
Binding site	CD*n*	Benzene	Pyrrole	Benzene	Pyrrole	Benzene	Pyrrole
II Trp99/Trp114*	3	4.09	4.42	3.34	4.07	135.3	104.5
	4	4.03	3.72	3.48	2.85	118.1	150.1
	5	4.10	4.00	3.35	3.57	136.3	109.8
	6	4.97	4.34	4.78	4.15	95.4	95.0
		4.93*	3.95*	4.15*	3.27*	139.0*	128.2*
III Trp147/Trp162*	3	3.70	4.25	2.95	3.93	134.6	102.4
	4	3.65	3.53	3.10	2.62	117.6	156.5
	5	3.83	3.97	3.15	3.69	128.4	99.5
	6	4.62	4.18	4.32	3.49	101.7	129.6
		3.85*	4.31*	2.97*	3.36*	151.3*	166.3*
VII Trp338/Trp354*	3	4.03	4.11	3.14	3.33	153.6	138.9
	4	4.46	4.01	4.27	3.37	95.3	125.2
	5	4.23	4.08	3.36	3.31	150.2	138.4
	6	5.32	4.81	5.13	4.58	96.0	98.0
		4.68*	3.71*	3.84*	3.00*	146.7*	130.8*

Distances d(C*n*-π) and d(D*n*-π) are measured from the carbon and deuterium atom, respectively, to the geometrical center of either the benzene or pyrrole aromatic rings of the tryptophan residue. Parameter ∠(C*n*-D*n*-π) is defined as an angle formed by carbon-deuterium-π center of the aromatic ring.

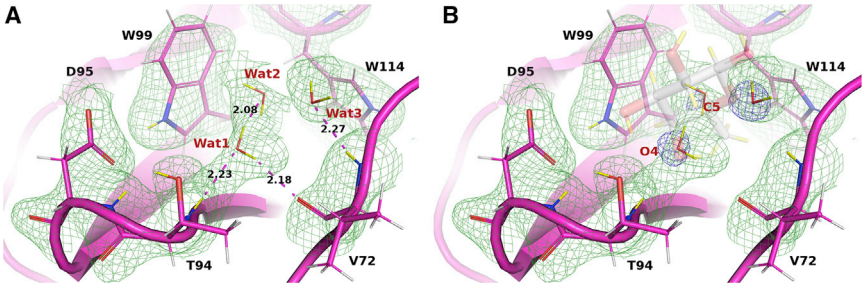

Figure 6. Water network in the binding site II of H/D-exchanged apo PLL

(A) Protein is depicted as magenta thin sticks. Hydrogen atoms are colored gray and deuterium atoms are colored yellow. Hydrogen bonds are shown as magenta dashed lines and distances are given in Å. The $2mF_o - DF_c$ neutron density map is shown as a green mesh and contoured at 1σ.

(B) Superposition of the water molecules and fucose (transparent gray sticks) in the binding site. The $2mF_o - DF_c$ electron density around water oxygen atoms is shown as a blue mesh and contoured at 1σ. The fucose atoms at the positions of water molecules are labeled.

interact with tryptophan residues using their O-H bonds or lone-pairs of electrons as described by NMR, molecular dynamics simulations, and quantum mechanics calculations (Durec et al., 2018; Špačková et al., 2018).

CONCLUSION

In this study, we reported two X-ray/neutron jointly refined structures of PLL lectin in apo form and in complex with perdeuterated L-fucose. The results show that NMX is a powerful technique for studying lectin-carbohydrate interactions since it can help resolve the complete hydrogen network in the ligand-binding sites as well as the directionality of water molecules involved in binding. We also described CD-π interactions that are crucial for the fucose specificity in the PLL lectin; this could be directly observed and their distances could be measured from the neutron structure. Finally, we have also observed an additional fucose-binding site from our X-ray structures showing that the number of PLL active sites is 4 per monomer and 16 per tetramer.

ACCESSION NUMBERS

The atomic coordinates and structure factors for the structures reported here have been deposited in the PDB under accession numbers PDB: 7BBI, 7BBC, 7B7F, 7B7E, 7B7C, and 7BB4.

STAR★METHODS

Detailed methods are provided in the online version of this paper and include the following:

- KEY RESOURCES TABLE
- RESOURCE AVAILABILITY
  - Lead contact
  - Materials availability
  - Data and code availability
- EXPERIMENTAL MODEL AND SUBJECT DETAILS
  - Bacterial cell culture
- METHOD DETAILS
  - Protein expression
  - Adaptation to D_2O and deuterated glycerol-d_8
  - Deuterated fed-batch fermentation
  - Protein purification
  - Production and purification of Fuc-d_{12}
  - Crystallization
  - Neutron data collection and processing
  - X-ray data collection and processing
  - Phasing and Structure refinement
- QUANTIFICATION AND STATISTICAL ANALYSIS

SUPPLEMENTAL INFORMATION

Supplemental information can be found online at https://doi.org/10.1016/j.str.2021.03.003.

ACKNOWLEDGMENTS

The authors wish to acknowledge the ESRF and ILL for provision of beamtime and technical support. We thank the ILL for the provision of studentship funding to L.G. V.T.F. acknowledges the UK Engineering and Physical Sciences Research Council (EPSRC) for grants GR/R99393/01 and EP/C015452/1 that funded the creation of the Deuteration Laboratory within ILL's Life Sciences Group. The authors acknowledge support from Glyco@Alps (ANR-15-IDEX02), Labex Arcane/CBH-EUR-GS (ANR-17-EURE-0003), and the Czech Ministry of Education, Youth and Sports (18-18964S). This work was supported by access to the HTX lab facility at EMBL and the PSB. We wish to acknowledge the IBS for access to the X-ray diffractometer and namely Florine Dupeux for help. We thank Nicolas Coquelle for help with the data collection and processing of X-ray data.

AUTHOR CONTRIBUTIONS

A.I., M.H., J.M.D., M.P.B., and V.T.F. designed the experiment. M.W. and A.K. provided expertise in the production and purification of the protein. L.G., J.M.D., M.H., and V.T.F. produced the deuterated biomolecules. L.G. purified the various components and carried out the experimental work. M.P.B. collected and processed the neutron data and provided expertise in structure determination. L.G. solved the crystal structures and refined them. L.G. prepared the figures and wrote the manuscript with A.I. and J.M.D., with critical inputs from all authors.

DECLARATION OF INTERESTS

The authors declare no competing interests.

Received: December 18, 2020
Revised: February 1, 2021
Accepted: March 3, 2021
Published: March 24, 2021

REFERENCES

Adams, P.D., Afonine, P.V., Bunkóczi, G., Chen, V.B., Davis, I.W., Echols, N., Headd, J.J., Hung, L.W., Kapral, G.J., Grosse-Kunstleve, R.W., et al. (2010). PHENIX: a comprehensive Python-based system for macromolecular structure solution. Acta Crystallogr. Sect. D Biol. Crystallogr. *66*, 213–221.

Afonine, P.V., Grosse-Kunstleve, R.W., Echols, N., Headd, J.J., Moriarty, N.W., Mustyakimov, M., Terwilliger, T.C., Urzhumtsev, A., Zwart, P.H., and

Adams, P.D. (2012). Towards automated crystallographic structure refinement with phenix. Refine. Acta Crystallogr. Sect. D Biol. Crystallogr. *68*, 352–367.

Artero, J.B., Härtlein, M., McSweeney, S., and Timmins, P. (2005). A comparison of refined X-ray structures of hydrogenated and perdeuterated rat γE-crystallin in H_2O and D_2O. Acta Crystallogr. Sect. D Biol. Crystallogr. *61*, 1541–1549.

Arzt, S., Campbell, J.W., Harding, M.M., Hao, Q., and Helliwell, J.R. (1999). Lscale—the new normalization, scaling and absorption correction program in the Daresbury Laue software suite. J. Appl. Crystallogr. *32*, 554–562.

Asensio, J.L., Ardá, A., Cañada, F.J., and Jiménez-Barbero, J. (2013). Carbohydrate-aromatic interactions. Acc. Chem. Res. *46*, 946–954.

Bacik, J.P., Mekasha, S., Forsberg, Z., Kovalevsky, A.Y., Vaaje-Kolstad, G., Eijsink, V.G.H., Nix, J.C., Coates, L., Cuneo, M.J., Unkefer, C.J., et al. (2017). Neutron and atomic resolution X-ray structures of a lytic polysaccharide monooxygenase reveal copper-mediated dioxygen binding and evidence for N-terminal deprotonation. Biochemistry *56*, 2529–2532.

Battye, T.G.G., Kontogiannis, L., Johnson, O., Powell, H.R., and Leslie, A.G.W. (2011). iMOSFLM: a new graphical interface for diffraction-image processing with MOSFLM. Acta Crystallogr. Sect. D Biol. Crystallogr. *67*, 271–281.

Beddoe, T., Paton, A.W., Le Nours, J., Rossjohn, J., and Paton, J.C. (2010). Structure, biological functions and applications of the AB5 toxins. Trends Biochem. Sci. *35*, 411–418.

Blakeley, M.P., Kalb, A.J., Helliwell, J.R., and Myles, D.A.A. (2004). The 15-K neutron structure of saccharide-free concanavalin A. Proc. Natl. Acad. Sci. U S A *101*, 16405–16410.

Blakeley, M.P., Teixeira, S.C.M., Petit-Haertlein, I., Hazemann, I., Mitschler, A., Haertlein, M., Howard, E., and Podjarny, A.D. (2010). Neutron macromolecular crystallography with LADI-III. Acta Crystallogr. Sect. D Biol. Crystallogr. *66*, 1198–1205.

Blakeley, M.P., Hasnain, S.S., and Antonyuk, S.V. (2015). Sub-atomic resolution X-ray crystallography and neutron crystallography: promise, challenges and potential. IUCrJ *2*, 464–474.

Blakeley, M.P., and Podjarny, A.D. (2018). Neutron macromolecular crystallography. Emerg. Top. Life Sci. *2*, 39–55.

Brandl, M., Weiss, M.S., Jabs, A., Sühnel, J., and Hilgenfeld, R. (2001). C-H···π-interactions in proteins. J. Mol. Biol. *307*, 357–377.

Campbell, J.W., Hao, Q., Harding, M.M., Nguti, N.D., Wilkinson, C., and IUCr. (1998). LAUEGEN version 6.0 and INTLDM. J. Appl. Crystallogr. *31*, 496–502.

Cress, B.F., Bhaskar, U., Vaidyanathan, D., Williams, A., Cai, C., Liu, X., Fu, L., M-Chari, V., Zhang, F., Mousa, S.A., et al. (2019). Heavy heparin: a stable isotope-enriched, chemoenzymatically-synthesized, poly-component drug. Angew. Chem. Int. Ed. Engl. *58*, 5962–5966.

Dimasi, N., Flot, D., Dupeux, F., and Márquez, J.A. (2007). Expression, crystallization and X-ray data collection from microcrystals of the extracellular domain of the human inhibitory receptor expressed on myeloid cells IREM-1. Acta Crystallogr. Sect. F Struct. Biol. Cryst. Commun. *63*, 204–208.

Durec, M., Marek, R., and Kozelka, J. (2018). Water-tryptophan interactions: lone-pair···π or O−H···π? Molecular dynamics simulations of β-galactosidase suggest that both modes can co-exist. Chemistry *24*, 5849–5859.

Emsley, P., Lohkamp, B., Scott, W.G., and Cowtan, K. (2010). Features and development of Coot. Acta Crystallogr. Sect. D Biol. Crystallogr. *66*, 486–501.

Eriksson, U.K., Fischer, G., Friemann, R., Enkavi, G., Tajkhorshid, E., and Neutze, R. (2013). Subangstrom resolution X-ray structure details aquaporin-water interactions. Science *340*, 1346–1349.

Evans, P. (2006). Scaling and assessment of data quality. Acta Crystallogr. Section D Biol. Crystallogr. *62*, 72–82.

Evans, P.R., and Murshudov, G.N. (2013). How good are my data and what is the resolution? Acta Crystallogr. Sect. D Biol. Crystallogr. *69*, 1204–1214.

Faltinek, L., Fujdiarová, E., Melicher, F., Houser, J., Kašáková, M., Kondakov, N., Kononov, L., Parkan, K., Vidal, S., and Wimmerová, M. (2019). Lectin PLL3, a novel monomeric member of the seven-bladed β-propeller lectin family. Molecules *24*, 4540.

Fisher, S.J., Blakeley, M.P., Howard, E.I., Petit-Haertlein, I., Haertlein, M., Mitschler, A., Cousido-Siah, A., Salvay, A.G., Popov, A., Muller-Dieckmann, C., et al. (2014). Perdeuteration: improved visualization of solvent structure in neutron macromolecular crystallography. Acta Crystallogr. Sect. D Biol. Crystallogr. *70*, 3266–3272.

Fujdiarová, E., Houser, J., Dobeš, P., Paulíková, G., Kondakov, N., Kononov, L., Hyršl, P., and Wimmerová, M. (2020). Heptabladed β-propeller lectins PLL2 and PHL from *Photorhabdus* spp. recognize *O*-methylated sugars and influence the host immune system. FEBS J. *288*, 1343–1365.

Gajdos, L., Forsyth, V.T., Blakeley, M.P., Haertlein, M., Imberty, A., Samain, E., and Devos, J.M. (2020). Production of perdeuterated fucose from glyco-engineered bacteria. Glycobiology *31*, 151–158.

Gerlits, O.O., Coates, L., Woods, R.J., and Kovalevsky, A. (2017). Mannobiose binding induces changes in hydrogen bonding and protonation states of acidic residues in concanavalin A as revealed by neutron crystallography. Biochemistry *56*, 4747–4750.

Habash, J., Raftery, J., Weisgerber, S., Cassetta, A., Lehmann, M.S., Høghøj, P., Wilkinson, C., Campbell, J.W., and Helliwell, J.R. (1997). Neutron Laue diffraction study of concanavalin A—the proton of Asp28. J. Chem. Soc. Faraday Trans. *93*, 4313–4317.

Habash, J., Raftery, J., Nuttall, R., Price, H.J., Wilkinson, C., Kalb, A.J., and Helliwell, J.R. (2000). Direct determination of the positions of the deuterium atoms of the bound water in concanavalin A by neutron Laue crystallography. Acta Crystallogr. Sect. D Biol. Crystallogr. *56*, 541–550.

Haertlein, M., Moulin, M., Devos, J.M., Laux, V., Dunne, O., and Forsyth, V.T. (2016). Biomolecular deuteration for neutron structural biology and dynamics. Methods Enzymol. *566*, 113–157.

Houser, J., Kozmon, S., Mishra, D., Mishra, S.K., Romano, P.R., Wimmerová, M., and Koca, J. (2017). Influence of trp flipping on carbohydrate binding in lectins. An example on *Aleuria aurantia* lectin AAL. PLoS One *12*, e0189375.

Houser, J., Kozmon, S., Mishra, D., Hammerová, Z., Wimmerová, M., and Koča, J. (2020). The CH–π interaction in protein–carbohydrate binding: bioinformatics and in vitro quantification. Chemistry *26*, 10769–10780.

Kabsch, W. (2010). XDS. Acta Crystallogr. D Biol. Crystallogr. *66*, 125–132.

Kalb, A.J., Habash, J., Hunter, N.S., Price, H.J., Raftery, J., and Helliwell, J.R. (2000). Manganese(II) in concanavalin A and other lectin proteins. Met. Ions Biol. Syst. *37*, 279–304.

Kent, B., Hauß, T., Demé, B., Cristiglio, V., Darwish, T., Hunt, T., Bryant, G., and Garvey, C.J. (2015). Direct comparison of disaccharide interaction with lipid membranes at reduced hydrations. Langmuir *31*, 9134–9141.

Koruza, K., Mahon, B.P., Blakeley, M.P., Ostermann, A., Schrader, T.E., McKenna, R., Knecht, W., and Fisher, S.Z. (2019). Using neutron crystallography to elucidate the basis of selective inhibition of carbonic anhydrase by saccharin and a derivative. J. Struct. Biol. *205*, 147–154.

Kovalevsky, A.Y., Katz, A.K., Carrell, H.L., Hanson, L., Mustyakimov, M., Zoe Fisher, S., Coates, L., Schoenborn, B.P., Bunick, G.J., Glusker, J.P., et al. (2008). Hydrogen location in stages of an enzyme-catalyzed reaction: time-of-flight neutron structure of D-xylose isomerase with bound D-xylulose. Biochemistry *47*, 7595–7597.

Kovalevsky, A.Y., Hanson, L., Fisher, S.Z., Mustyakimov, M., Mason, S.A., Trevor Forsyth, V., Blakeley, M.P., Keen, D.A., Wagner, T., Carrell, H.L., et al. (2010). Metal ion roles and the movement of hydrogen during reaction catalyzed by D-xylose isomerase: a joint X-ray and neutron diffraction study. Structure *18*, 688–699.

Kumar, A., Sýkorová, P., Demo, G., Dobeš, P., Hyršl, P., and Wimmerová, M. (2016). A novel fucose-binding lectin from *Photorhabdus luminescens* (PLL) with an unusual heptabladed β-propeller tetrameric structure. J. Biol. Chem. *291*, 25032–25049.

Langan, P., Sangha, A.K., Wymore, T., Parks, J.M., Yang, Z.K., Hanson, B.L., Fisher, Z., Mason, S.A., Blakeley, M.P., Forsyth, V.T., et al. (2014). L-Arabinose binding, isomerization, and epimerization by D-xylose isomerase: X-ray/neutron crystallographic and molecular simulation study. Structure *22*, 1287–1300.

Lis, H., and Sharon, N. (1998). Lectins: carbohydrate-specific proteins that mediate cellular recognition. Chem. Rev. *98*, 637–674.

Machado, R.A.R., Wüthrich, D., Kuhnert, P., Arce, C.C.M., Thönen, L., Ruiz, C., Zhang, X., Robert, C.A.M., Karimi, J., Kamali, S., et al. (2018). Whole-genome-based revisit of *Photorhabdus* phylogeny: proposal for the elevation of most *Photorhabdus* subspecies to the species level and description of one novel species *Photorhabdus bodei* sp. nov., and one novel subspecies *Photorhabdus laumondii* subsp. *clarkei* subsp. nov. Int. J. Syst. Evol. Microbiol. *68*, 2664–2681.

Maeki, M., Ito, S., Takeda, R., Ueno, G., Ishida, A., Tani, H., Yamamoto, M., and Tokeshi, M. (2020). Room-temperature crystallography using a microfluidic protein crystal array device and its application to protein-ligand complex structure analysis. Chem. Sci. *11*, 9072–9087.

Manzoni, F., Saraboji, K., Sprenger, J., Kumar, R., Noresson, A.L., Nilsson, U.J., Leffler, H., Fisher, S.Z., Schrader, T.E., Ostermann, A., et al. (2016). Perdeuteration, crystallization, data collection and comparison of five neutron diffraction data sets of complexes of human galectin-3C. Acta Crystallogr. Sect. D Struct. Biol. *72*, 1194–1202.

Manzoni, F., Wallerstein, J., Schrader, T.E., Ostermann, A., Coates, L., Akke, M., Blakeley, M.P., Oksanen, E., and Logan, D.T. (2018). Elucidation of hydrogen bonding patterns in ligand-free, lactose- and glycerol-bound galectin-3C by neutron crystallography to guide drug design. J. Med. Chem. *61*, 4412–4420.

McCoy, A.J., Grosse-Kunstleve, R.W., Adams, P.D., Winn, M.D., Storoni, L.C., and Read, R.J. (2007). Phaser crystallographic software. J. Appl. Crystallogr. *40*, 658–674.

Meilleur, F., Weiss, K.L., and Myles, D.A.A. (2009). Deuterium labeling for neutron structure-function-dynamics analysis. Methods Mol. Biol. *544*, 281–292.

Moonens, K., and Remaut, H. (2017). Evolution and structural dynamics of bacterial glycan binding adhesins. Curr. Opin. Struct. Biol. *44*, 48–58.

Moriarty, N.W., Grosse-Kunstleve, R.W., and Adams, P.D. (2009). Electronic ligand builder and optimization workbench (eLBOW): a tool for ligand coordinate and restraint generation. Acta Crystallogr. Sect. D Biol. Crystallogr. *65*, 1074–1080.

Mousavifar, L., Touaibia, M., and Roy, R. (2018). Development of mannopyranoside therapeutics against adherent-invasive *Escherichia coli* infections. Acc. Chem. Res. *51*, 2937–2948.

Niimura, N., Minezaki, Y., Nonaka, T., Castagna, J.C., Cipriani, F., Høghøj, P., Lehmann, M.S., and Wilkinson, C. (1997). Neutron Laue diffractometry with an imaging plate provides an effective data collection regime for neutron protein crystallography. Nat. Struct. Biol. *4*, 909–914.

O'Dell, W.B., Agarwal, P.K., and Meilleur, F. (2017). Oxygen activation at the active site of a fungal lytic polysaccharide monooxygenase. Angew. Chem. Int. Ed. Engl. *56*, 767–770.

Regaiolo, A., Dominelli, N., Andersen, K., and Heermann, R. (2020). The biocontrol agent and insect pathogen *Photorhabdus luminescens* interacts with plant roots. Appl. Env. Microb. *86*, e00891–20.

Ryu, K.S., Kim, C., Park, C., and Choi, B.S. (2004). NMR analysis of enzyme-catalyzed and free-equilibrium mutarotation kinetics of monosaccharides. J. Am. Chem. Soc. *126*, 9180–9181.

Sawama, Y., Yabe, Y., Iwata, H., Fujiwara, Y., Monguchi, Y., and Sajiki, H. (2012). Stereo- and regioselective direct multi-deuterium-labeling methods for sugars. Chemistry *18*, 16436–16442.

Schirò, G., Vetri, V., Frick, B., Militello, V., Leone, M., and Cupane, A. (2012). Neutron scattering reveals enhanced protein dynamics in concanavalin A amyloid fibrils. J. Phys. Chem. Lett. *3*, 992–996.

Špačková, N., Trošanová, Z., Šebesta, F., Jansen, S., Burda, J.V., Srb, P., Zachrdla, M., Žídek, L., and Kozelka, J. (2018). Protein environment affects the water-tryptophan binding mode. MD, QM/MM, and NMR studies of engrailed homeodomain mutants. Phys. Chem. Chem. Phys. *20*, 12664–12677.

Takaba, K., Tai, Y., Eki, H., Dao, H.-A., Hanazono, Y., Hasegawa, K., Miki, K., and Takeda, K. (2019). Subatomic resolution X-ray structures of green fluorescent protein. IUCrJ *6*, 387–400.

Thaller, C., Weaver, L.H., Eichele, G., Wilson, E., Karlsson, R., and Jansonius, J.N. (1981). Repeated seeding technique for growing large single crystals of proteins. J. Mol. Biol. *147*, 465–469.

Wan, Q., Parks, J.M., Hanson, B.L., Fisher, S.Z., Ostermann, A., Schrader, T.E., Graham, D.E., Coates, L., Langan, P., and Kovalevsky, A. (2015). Direct determination of protonation states and visualization of hydrogen bonding in a glycoside hydrolase with neutron crystallography. Proc. Natl. Acad. Sci. U S A *112*, 12384–12389.

Waterfield, N.R., Ciche, T., and Clarke, D. (2009). *Photorhabdus* and a host of hosts. Annu. Rev. Microbiol. *63*, 557–574.

Williams, C.J., Headd, J.J., Moriarty, N.W., Prisant, M.G., Videau, L.L., Deis, L.N., Verma, V., Keedy, D.A., Hintze, B.J., Chen, V.B., et al. (2018). MolProbity: more and better reference data for improved all-atom structure validation. Protein Sci. *27*, 293–315.

Wimmerová, M., Kozmon, S., Nečasová, I., Mishra, S.K., Komárek, J., and Koča, J. (2012). Stacking interactions between carbohydrate and protein quantified by combination of theoretical and experimental methods. PLoS One *7*, e46032.

Winn, M.D., Ballard, C.C., Cowtan, K.D., Dodson, E.J., Emsley, P., Evans, P.R., Keegan, R.M., Krissinel, E.B., Leslie, A.G.W., McCoy, A., et al. (2011). Overview of the CCP4 suite and current developments. Acta Crystallogr. Sect. D Biol. Crystallogr. *67*, 235–242.

Woińska, M., Grabowsky, S., Dominiak, P.M., Woźniak, K., and Jayatilaka, D. (2016). Hydrogen atoms can be located accurately and precisely by x-ray crystallography. Sci. Adv. *2*, e1600192.

Please cite this article in press as: Gajdos et al., Visualization of hydrogen atoms in a perdeuterated lectin-fucose complex reveals key details of protein-carbohydrate interactions, Structure (2021), https://doi.org/10.1016/j.str.2021.03.003

STAR★METHODS

KEY RESOURCES TABLE

REAGENT or RESOURCE	SOURCE	IDENTIFIER
Bacterial and Virus Strains		
Escherichia coli BL21(DE3)	Invitrogen / Life technologies	Cat#C600003
Chemicals, Peptides, and Recombinant Proteins		
L-fucose	Carbosynth	Cat#MF06710 CAS: 2438-80-4
Perdeuterated L-Fucose	(Gajdos et al., 2020)	N/A
Recombinant PLL	(Kumar et al., 2016)	N/A
Deuterated recombinant PLL	This paper	N/A
Deposited Data		
X-ray/neutron RT H/D-exchanged apo PLL	This paper	PDB: 7BBI
X-ray/neutron RT D-PLL/Fuc-d_{12}	This paper	PDB: 7BBC
X-ray RT D-PLL apo	This paper	PDB: 7B7E
X-ray RT H/D-exchanged PLL/H-fucose	This paper	PDB: 7B7F
X-ray RT D-PLL/H-fucose	This paper	PDB: 7B7C
X-ray 100 K D-PLL/H-fucose	This paper	PDB: 7BB4
Coordinates of rPLL	(Kumar et al., 2016)	PDB: 5C9O
Coordinates of rPLL in the presence of L-fucose	(Kumar et al., 2016)	PDB: 5C9P
Recombinant DNA		
Plasmid pET29a	Novagen	Cat#69871
Plasmid pET29a-pll	(Kumar et al., 2016)	N/A
Software and Algorithms		
XDS	(Kabsch, 2010)	http://www.xds.mpimf-heidelberg.mpg.de/
Phenix 1.16.3	(Adams et al., 2010)	https://www.phenix-online.org/
CCP4	(Winn et al., 2011)	http://www.ccp4.ac.uk
Coot	(Emsley et al., 2010)	https://bernhardcl.github.io/coot
Molprobity	(Williams et al., 2018)	http://molprobity.biochem.duke.edu/
Pymol 2.3.2	Schrodinger, LLC	https://pymol.org/2/
iMosflm	(Battye et al., 2011)	http://www.ccp4.ac.uk
LAUEGEN	(Campbell et al., 1998)	https://web.archive.org/web/20001024010254/http://www.dl.ac.uk/SRS/PX/jwc_laue/laue_top.html
LSCALE	(Arzt et al., 1999)	https://web.archive.org/web/20001024010254/http://www.dl.ac.uk/SRS/PX/jwc_laue/laue_top.html

RESOURCE AVAILABILITY

Lead contact

Further information and requests for resources and reagents should be directed to and will be fulfilled by the lead contact, Anne Imberty (anne.imberty@cermav.cnrs.fr).

Materials availability

This study did not generate new unique reagent.

Data and code availability

Model coordinates and experimental data have been deposited in the Protein Data Bank under PDB accession codes for jointly refined X-ray/neutron structures PDB: 7BBI for H/D-exchanged apo PLL structure, PDB: 7BBC for the D-PLL/Fuc-d_{12} complex. In

addition, the following X-ray structures have also been deposited: PDB: 7B7F for H/D-PLL complexed with H-fucose at room temperature, PDB: 7B7E for D-PLL apo at room temperature, PDB: 7B7C for D-PLL complexed with H-fucose at room temperature, and PDB: 7BB4 for D-PLL complexed with H-fucose at 100K.

EXPERIMENTAL MODEL AND SUBJECT DETAILS

Bacterial cell culture

Both hydrogenated and perdeuterated PLL lectin were expressed in *Escherichia coli* BL21(DE3) cells using pET-29a-*pll* (Kumar et al., 2016) under kanamycin selection. All culture media were supplemented with 35 μg mL^{-1} kanamycin and grown at 37°C with shaking at 180 rpm.

METHOD DETAILS

Protein expression

The hydrogenated protein was produced in LB medium as described previously (Kumar et al., 2016). Briefly, *E. coli* BL21(DE3) cells containing pET29a-*pll* plasmid were cultured in LB medium with 35 μg mL^{-1} kanamycin at 37°C until OD_{600} of 0.6-0.8. The protein expression was induced with IPTG (0.2 mM) and the cells were grown at 25°C for 12 h. The cells were harvested (8000 rpm at 4°C for 1 h) and the cell paste was frozen at -80°C.

Adaptation to D_2O and deuterated glycerol-d_8

The *E. coli* cells containing pET29a-*pll* plasmid (Kumar et al., 2016) were adapted to fully deuterated Enfors minimal medium with a define composition as previously described (Artero et al., 2005; Haertlein et al., 2016) with the following composition: 6.86 g L^{-1} $(NH_4)_2SO_4$, 1.56 g L^{-1} KH_2PO_4, 6.48 g L^{-1} $Na_2HPO_4 \cdot 2H_2O$, 0.49 g L^{-1} $(NH_4)_2HC_6H_5O_7$ (diammonium hydrogen citrate), 0.25 g L^{-1} $MgSO_4 \cdot 7H_2O$, with 1.0 mL L^{-1} of trace metal stock solution (0.5 g L^{-1} $CaCl_2 \cdot 2H_2O$, 16.7 g L^{-1} $FeCl_3 \cdot 6H_2O$, 0.18 g L^{-1} $ZnSO_4 \cdot 7H_2O$, 0.16 g L^{-1} $CuSO_4 \cdot 5H_2O$, 0.15 g L^{-1} $MnSO_4 \cdot 4H_2O$, 0.18 g L^{-1} $CoCl_2 \cdot 6H_2O$, 20.1 g L^{-1} EDTA), 5 g L^{-1} glycerol-d_8. A single colony of *E. coli* containing pET29a-*pll* plasmid grown overnight on an LB agar plate supplemented with kanamycin was used to inoculate 15 mL of hydrogenated Enfors minimal medium and was grown overnight at 37°C. The culture was then used to inoculate 15 mL of 100% D_2O Enfors minimal medium (with deuterated glycerol-d_8) at OD_{600} of 0.1 and was grown overnight at 37°C. This passaging step was repeated five times until the doubling time for *E. coli* reached values similar to those for hydrogenated cultures.

Deuterated fed-batch fermentation

A deuterium-adapted preculture of 150 mL was used to inoculate 1.2 L of the fully deuterated Enfors minimal medium described above in a 3 L bioreactor (Infors AG, Switzerland) used for fed-batch fermentation. The pD of the culture medium was maintained at 7.2 by addition of 4% NaOD and the temperature at 30°C. After exhaustion of glycerol-d_8 (Euriso-top, France) from the culture medium, the fed-batch phase was initiated by continuous exponential feeding with additional 30 g of glycerol-d_8. PLL expression was induced with 1 mM isopropyl-β-D-thiogalactopyranoside (IPTG) at OD_{600} of 16 and harvested after 19 h induction by centrifugation (8000 g for 1 h at 4°C). The cell paste was frozen at -80°C for long-term storage. The cell paste yield was 66 g wet weight from a 1.8-liter culture.

Protein purification

Both hydrogenated and perdeuterated PLL were purified the same way using Ni^{2+} affinity chromatography (AKTA Prime) and hydrogenated buffers. The cell paste was resuspended in lysis buffer (20 mM potassium phosphate pH 7.5, 2 mM trehalose) in the presence of EDTA-free protease inhibitor cocktail (Roche, Mannheim, Germany). The cells were lysed by cell disruption at a pressure of 1.8 Kbar (Constant Systems Ltd, UK). After centrifugation (24 000 g for 40 min at 4°C), the supernatant was filtered (0.45 μm) and the cleared cell lysate was loaded onto a His Trap FF column (GE Healthcare Life Sciences (now Cytiva), USA) pre-equilibrated with the lysis buffer. Protein was eluted using phosphate buffer containing 100 mM imidazole. The purity of the protein was verified by 12% Tris-Tricine SDS-PAGE stained with Coomassie Blue. The protein MW estimated from SDS-PAGE was about 40 kDa for both proteins, in agreement with the theoretical MW of 41.9 kDa. Fractions containing pure protein were pooled together and dialyzed against the lysis buffer and concentrated using 30-kDa MW cut-off centrifugal filter units (Amicon, Merck Millipore). The concentrated protein was flash-frozen in small aliquots of 200 μL in liquid nitrogen for long-term storage. The typical yield of perdeuterated PLL lectin was about 4 mg of protein per 1 g of wet cell paste.

Production and purification of Fuc-d_{12}

The fully-deuterated fucose (Fuc-d_{12}) was produced using glyco-engineered bacteria in a bioreactor as described previously (Gajdos et al. 2020). The secreted fully-deuterated fucose was further purified and characterised before being used for the crystallisation experiments described in this work.

Please cite this article in press as: Gajdos et al., Visualization of hydrogen atoms in a perdeuterated lectin-fucose complex reveals key details of protein-carbohydrate interactions, Structure (2021), https://doi.org/10.1016/j.str.2021.03.003

Crystallization

Crystallization experiments were carried out at the High Throughput Crystallisation Laboratory (HTX Lab) of the EMBL Grenoble (Dimasi et al., 2007). Both hydrogenated and deuterated PLL lectin were crystallized using vapour-diffusion sitting drop method in 24-well crystallization plates (Hampton Research, USA) in the following three conditions: 0.1 M sodium acetate, pD 4.6, 8% (w/v) polyethylene glycol (PEG) 4000; 0.1 M Tris-DCl, pD 8.5, 6-8% (w/v) PEG 8 000; 0.05-0.4 M sodium-potassium tartrate. The final volume of the drops was 8-16 μL, the protein : reservoir ratio was 3:1 and the volume of the reservoir solution was 0.5 mL. Crystallization plates were incubated at 18°C. Hydrogenated crystals used for neutron diffraction experiments were H/D-exchanged by vapour diffusion. Reservoir solution was replaced by deuterated solution in a stepwise manner starting from 25% to 100% deuterated solution over a period of two weeks.

Crystals of deuterated PLL lectin in complex with deuterated fucose-d_{12} were obtained in the following conditions: 0.05-0.1 M sodium-potassium tartrate. Crystals were either co-crystallized or soaked with Fuc-d_{12} to a final concentration of 50 mM. All solutions were dissolved in D_2O. A macro-seeding technique was applied to grow large crystals for neutron diffraction experiments (Thaller et al., 1981). Crystals of 0.05-0.1 mm^3 were harvested and introduced into pre-equilibrated drops containing the protein solution. Crystals were growing for several weeks. In order to avoid damaging the crystals by repeated seeding, crystals were regularly fed with fresh protein solution. The lid was open once per week and 3-4 μL of a pre-equilibrated protein solution was added onto the drop. Final volumes of crystals obtained using this method were 0.5-0.7 mm^3. To exchange all labile hydrogens that might have been back-exchanged when the sitting-drop lid was open, the reservoir solution was replaced for freshly-prepared deuterated solution three times prior to crystal mounting in quartz capillaries.

Neutron data collection and processing

Crystals of PLL lectin were mounted either in thin (0.01 mm thickness, Hampton Research, US) or thick-walled quartz capillaries (0.2 mm thickness, Vitrocom from CM Scientific, UK) with inner diameter 1.5-2.0 mm and sealed with wax in preparation for data collection at room-temperature using the LADI-III diffractometer at the Institut Laue-Langevin (Blakeley et al., 2010). Using a neutron wavelength range from 3.1-4.1 Å, neutron diffraction data extending to 2.2 Å resolution were collected for D-PLL complexed with Fuc-d_{12} and for H/D-exchanged apo PLL. The neutron diffraction data for the D-PLL/Fuc-d_{12} complex were collected from a single crystal with volume of 0.5 mm^3 using 18h exposures. Nineteen images were collected from two different crystal orientations. The neutron diffraction data for H/D-exchanged apo PLL were collected from two crystals with volumes of ~0.7 mm^3 that had been grown in the same crystallization condition. Ten images (each of 18h) were collected in total from the two crystals. Neutron data were indexed and integrated using *LAUEGEN* (Campbell et al., 1998), wavelength normalized using *LSCALE* (Arzt et al., 1999) and merged using *SCALA* (Evans, 2006). Complete data collection and structure refinement statistics are presented in Table S1.

X-ray data collection and processing

Room temperature (RT) X-ray datasets were collected for both crystals from which the neutron data were collected. For the H/D-exchanged apo PLL crystal, the data images were recorded on the BM30A (newly BM07) beamline at the ESRF (Grenoble, France). The same beamline was used to collect RT datasets of H/D-PLL-H-fucose, D-PLL apo and D-PLL-H-fucose crystals (hydrogenated commercial L-fucose was used for the crystals). The collected data were processed using *XDS* (Kabsch, 2010), scaled and merged in *AIMLESS* (Evans and Murshudov, 2013) and converted to structure factors using *TRUNCATE* from the *CCP4* program suite (Winn et al., 2011). For the D-PLL-Fuc-d_{12} crystal, the RT X-ray datasets were recorded on the GeniX 3D Cu High Flux diffractometer (Xenocs) at the IBS, Grenoble, France. Data were integrated using *iMOSFLM* (Battye et al., 2011), scaled and merged using *AIMLESS* and converted to structure factors using *TRUNCATE* from the *CCP4* program suite.

To collect the 100 K X-ray data, crystals were cryo-protected by soaking in 30% (v/v) glycerol in a crystallization solution for a time as short as possible and were subsequently cryo-cooled at 100 K in liquid nitrogen. Datasets from crystals of D-PLL/H-fucose complex were collected on the ID23-1 beamline at the ESRF equipped with the PILATUS 6M detector. The data were processed via XIA2 pipeline. Complete data collection and structure refinement statistics are presented in Table S2.

Phasing and Structure refinement

Monomeric structure of the recombinant PLL lectin (PDB: 5C9O) stripped of water molecules was used as the initial model for initial phasing using molecular replacement (McCoy et al., 2007). Crystallographic refinement was carried out with *phenix.refine* (Afonine et al., 2012) from the *PHENIX* package (Adams et al., 2010) altered with a manual model building and model adjustments using *Coot* (Emsley et al., 2010). Water molecules were introduced automatically using *phenix.refine* and inspected manually. Ligand molecules were introduced manually in *Coot*.

The joint x-ray/neutron refinement was carried out after the satisfactory R factors were achieved. The final X-ray and neutron R_{work}/R_{free} values for the H/D-exchanged apo PLL were 13.5%/15.6% and 21.5%/24.0% respectively and for the D-PLL/Fuc-d_{12} complex were 12.1%/14.0% and 19.2%/22.3% respectively. The *ReadySet* utility in *PHENIX* was used to introduce hydrogen and deuterium atoms at appropriate positions in the protein and ligand molecules. The *eLBOW* (Moriarty et al., 2009) tool in *PHENIX* was used to generate restraint files for the hydrogenated and deuterated fucose molecules. Molecular figures were prepared in *PyMOL* (Schrödinger, Inc.). Complete data collection and structure refinement statistics are presented in Tables 1, S1 and S2.

QUANTIFICATION AND STATISTICAL ANALYSIS

Processing of X-ray and neutron data was performed as described in the Method Details. Model refinement was carried out in *Phenix* using *phenix.refine* (Afonine et al., 2012). All software used is listed in the Key resources table. Data processing, refinement, and validation statistics are summarized in Tables 1, S1 and S2. Structure validation was performed on the deposited atomic models using *Molprobity* (Williams et al., 2018).